

Evaluation of torsional response of a long-span suspension bridge under railway traffic and typhoons based on SHM data

Yun-Xia Xia^a, Yi-Qing Ni^{*} and Chi Zhang^b

*Department of Civil and Environmental Engineering, The Hong Kong Polytechnic University,
Hung Hom, Kowloon, Hong Kong*

(Received June 12, 2014, Revised September 28, 2014, Accepted October 1, 2014)

Abstract. Long-span cable-supported bridges are flexible structures vulnerable to unsymmetric loadings such as railway traffic and strong wind. The torsional dynamic response of long-span cable-supported bridges under running trains and/or strong winds may deform the railway track laid on the bridge deck and affect the running safety of trains and the comfort of passengers, and even lead the bridge to collapse. Therefore, it is eager to figure out the torsional dynamic response of long-span cable-supported bridges under running trains and/or strong winds. The Tsing Ma Bridge (TMB) in Hong Kong is a suspension bridge with a main span of 1,377 m, and is currently the world's longest suspension bridge carrying both road and rail traffic. Moreover, this bridge is located in one of the most active typhoon-prone regions in the world. A wind and structural health monitoring system (WASHMS) was installed on the TMB in 1997, and after 17 years of successful operation it is still working well as desired. Making use of one-year monitoring data acquired by the WASHMS, the torsional dynamic responses of the bridge deck under rail traffic and strong winds are analyzed. The monitoring results demonstrate that the differences of vertical displacement at the opposite edges and the corresponding rotations of the bridge deck are less than 60 mm and 0.1° respectively under weak winds, and less than 300 mm and 0.6° respectively under typhoons, implying that the torsional dynamic response of the bridge deck under rail traffic and wind loading is not significant due to the rational design.

Keywords: torsional response; long-span suspension bridge; railway traffic; typhoon; structural health monitoring

1. Introduction

Long-span cable-supported bridges are flexible structures susceptible to various types of loads such as highway and railway traffic and winds. Heavy trains running deviating from the longitudinal central line of the deck generate eccentric forces acting on the deck which would induce torsional response of the bridge. If a long-span railway bridge is built in a wind prone area, the bridge will also experience torsional vibration due to aerodynamic effects. The torsional vibration of the bridge due to running trains or strong winds or both may deform the railway track

*Corresponding author, Professor, E-mail: ceyqni@polyu.edu.hk

^a Ph.D. Student, E-mail: yunxia.xia@connect.polyu.hk

^b M.Sc. Student, E-mail: zc.zhang@connect.polyu.hk

laid on the bridge deck and affect the running safety of trains and the comfort of passengers, and even make the bridge collapse. On 7 November 1940, the Tacoma Narrows suspension bridge in Washington State, USA, collapsed four months after its opening due to a gale with wind speeds reaching 19 m/s. The collapse of the bridge followed 70 minutes of violent oscillatory motion of the deck, during which the cross sections at the quarter points of the main span twisted with angle amplitudes of approximately $\pm 35^\circ$ (Larsen 2000). Therefore, it is desirable to understand the torsional dynamic behavior of long-span cable-supported bridges under running trains and strong winds. Previous research focused on the establishment and verification of analytical models to study the dynamic response such as vertical acceleration and displacement and lateral acceleration and displacement of long cable-supported bridges under railway traffic (Diana and Cheli 1989, Fryba 1996, Kwark *et al.* 2004, Lee *et al.* 2005, Zhang *et al.* 2013), strong winds (Scanlan 1978, Scanlan and Jones 1990, Pfeil and Batista 1995, Larose and Livesey 1997, Boonyapinyo 1999, Chen *et al.* 2000, Ding *et al.* 2000, Chen and Kareem 2003, Diana *et al.* 2010, Wu and Kareem 2013) or both strong wind and railway traffic (Cai and Chen 2004, Xu *et al.* 2007, Xia *et al.* 2008, Guo *et al.* 2011). However, there was no detailed and systematic study on the torsional dynamic response of long-span cable-supported bridges under railway traffic and strong winds based on long-term in-situ monitoring data which are expected to provide more authentic information about the wind and railway traffic loading and bridge behavior.

The Tsing Ma Bridge (TMB) in Hong Kong is a long-span steel suspension bridge with a main span length of 1,377 m, and is currently the world's longest suspension bridge carrying both road and rail traffic. Since the TMB is located in a typhoon region and subjected to both highway and railway traffic loadings, the torsional dynamic response of the deck must be concerned. The TMB was installed with a long-term structural health monitoring system called WASHMS in 1997 (Wong 2004, Wong 2007, Ni *et al.* 2011). The WASHMS is composed of around 300 sensors in eight types, namely, anemometers, servo-type accelerometers, temperature sensors, welded foil-type strain gauges (or dynamic strain gauges), global positioning systems (GPS), displacement transducers, level sensing stations, and dynamic weigh-in-motion stations, for the purpose of monitoring the load conditions such as highway and railway traffic and winds, environmental factors such as temperature, and structural response such as acceleration, displacement and strain continuously. After continuous operation for 17 years, the WASHMS is still working well. With one-year continuously monitored data by the WASHMS, the torsional dynamic responses of the bridge deck under railway traffic and typhoons are explored in this study. The one-year data are classified into two sets: the first set is the data under weak wind condition (hourly average wind speed less than 2 m/s), and the second set is the data under typhoon condition. For each data set, three railway loading cases are considered: (i) no train on the bridge; (ii) one train running on the bridge; and (iii) two trains running in opposite directions on the bridge. The wind conditions are determined by the wind speed measured by the anemometers deployed on the bridge; and the number of trains running on the bridge, and the speed and location of the train are identified using the measured data from strain gauges near the railway tracks. The relative vertical displacement at the opposite edges of the bridge deck with respect to the longitudinal central axis and the rotation of the bridge deck are analyzed based on the measured data from the level sensing stations, GPS and accelerometers.

2. Tsing Ma Bridge

2.1 Structural features

The Tsing Ma Bridge (TMB) is the key linkage of the most important transport network in Hong Kong which connects the international airport to the commercial centers. It is a long-span suspension bridge with a total length of 2,132 m and a main span of 1,377 m between the Tsing Yi tower in the east and the Ma Wan tower in the west, making it currently the world's longest suspension bridge carrying both highway and railway traffic. The two concrete towers are 206 m high measured from the base level to the tower saddle. The two anchorages are gravity structures designed with a minimum safety factor of two against sliding over or shearing through the underlying rock. The upper parts of the anchorages form the deck abutments. The two main cables of 36 m apart in the north and south are accommodated by four saddles at the top of the tower legs. The deck of the TMB has two levels (the upper level carries a dual three-lane highway and the lower level carries two railway tracks and two single-lane carriage ways), and a minimum of 62.1 m to shipping channel below (Beard and Young 1995). The layout of the TMB is shown in Fig. 1(a).

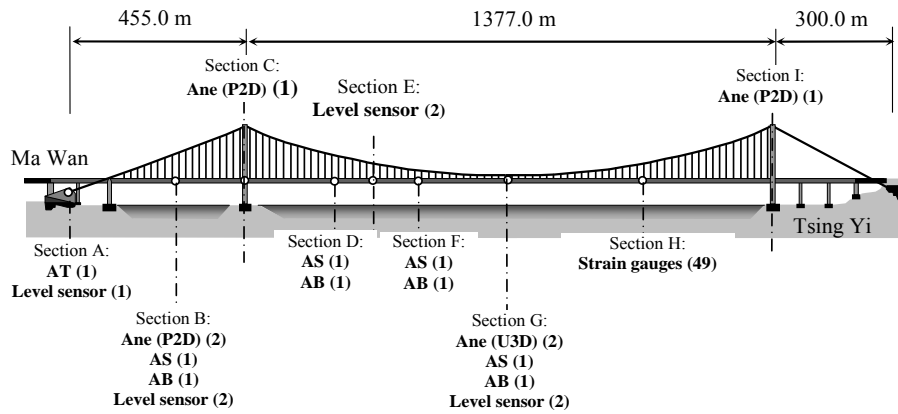
The key structural feature of the TMB is the stiffening deck system which is a streamlined box-shaped steel truss girder with central air-gap. The truss girder has two types of trusses, i.e., the Warren truss in the longitudinal direction, and the Vierendeel truss in the transverse direction. The adoption of streamlined shape and central air-gap is to minimize the wind dragging forces acting on the bridge deck and to increase the aerodynamic stability of the stiffening deck system under high wind speeds. The two longitudinal trusses link up the cross frames with 4.5 m apart from each other along the bridge longitudinal axis, acting as the main girder of the bridge. As shown in Figs. 1(b)-1(c), each longitudinal truss is composed of upper, lower, vertical and diagonal chords; and each cross frame comprises upper and lower chords, inner struts, outer struts (also the vertical members of the longitudinal trusses), and upper and lower inclined edge members. At the main span and the Ma Wan side span, the deck is suspended from the main cables at 18 m intervals, i.e., at every four cross frames; and at the Ma Wan tower and the Tsing Yi tower, it is supported by rocker bearings and sliding bearings, respectively.

2.2 Train and wind characteristics

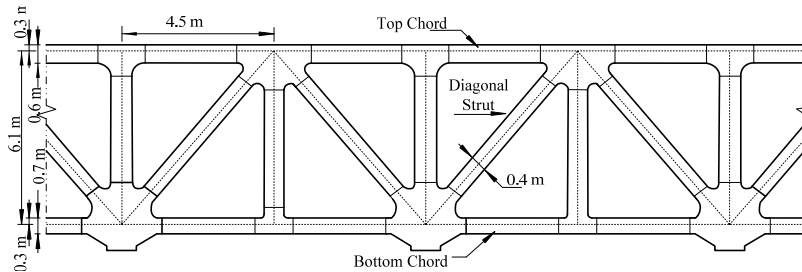
There are two railway tracks close to the longitudinal central axis of the bottom deck, on the north and south sides, respectively (see Fig. 1(c)). The north track is directed from Ma Wan to Tsing Yi while the south track is directed from Tsing Yi to Ma Wan. This passenger railway began to operate in June 1998. Before 2003 most trains passing through the TMB were 7-car trains, however, with the increasing demand of passenger flow, most trains had become 8-car trains (see Fig. 2) since the end of 2005. The years between 2003 and 2005 were a transition period with 7-car and 8-car trains running concurrently. The full length of a carriage is about 22.5 m, so the total length of a 7-car and 8-car train is approximately 158 m and 182 m, respectively (Xu *et al.* 2007). Each carriage has two identical bogies, each of which is supported by two identical wheel sets. The running speed of the trains is about 30 m/s; as a result, it takes about 1.5 minutes for a train to pass through the whole bridge. The design railway loading for the TMB is based on an 8-car train, and for static design the maximum axle loading was taken as 17 tons whereas for fatigue effects a 13 tons axle loading was adopted with an annual tonnage of 51 million tons per

tack. The passing rate of the twin track railway was assessed at 10% (Beard and Young 1995).

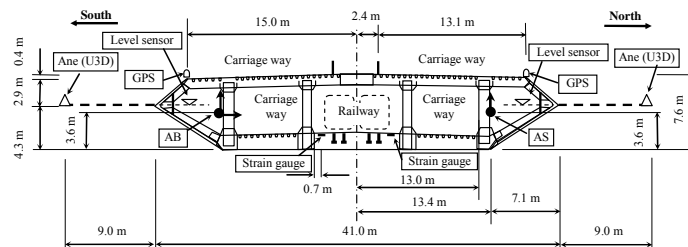
Hong Kong is located in the southern coast of China and is within the Pacific Typhoon Belt, one of the most active typhoon-prone regions in the world. Based on the typhoon record provided by the Hong Kong Observatory, almost every year there are several strong typhoons striking Hong Kong, and there have been 54 typhoons with signal no less than eight, which refers to gale with a sustained wind speed of 63 to 117 km/h from the quarter indicated and gusts which may exceed 180 km/h (HKO 2014). In addition, Hong Kong greatly suffers the influence of prevailing monsoon winds in both winter and summer due to the difference in temperature and pressure gradient.



(a) Layout of TMB and locations of sensors



(b) Longitudinal truss



(c) Transverse truss and locations of typical sensors

Fig. 1 Layout of TMB, longitudinal and transverse trusses, and locations of typical sensors

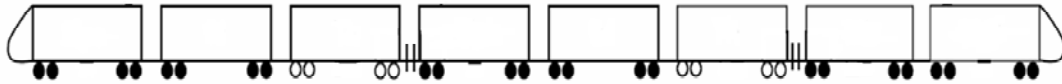


Fig. 2 Configuration of 8-car train

3. Wind and structural health monitoring system

A long-term monitoring system called Wind And Structural Health Monitoring System (WASHMS) was deployed and implemented on the TMB in 1997 to monitor and evaluate the structural health of the bridge under in-service condition (Wong 2004, Wong 2007, Ni *et al.* 2011). The objectives of the WASHMS are: (i) to monitor and evaluate the structural health of the bridge; (ii) to provide information for the planning of inspection and maintenance activities; and (iii) to verify design assumptions and parameters for future design and construction of similar bridges around Hong Kong. The WASHMS is composed of about 300 sensors in eight types, namely, anemometers, servo-type accelerometers, temperature sensors, welded foil-type strain gauges (or dynamic strain gauges), global positioning systems (GPS), displacement transducers, level sensing stations, and dynamic weigh-in-motion stations.

Two types of anemometers are deployed on the tower top and deck level: tri-axial ultrasonic anemometer (Ane (U3D)) and propeller anemometer (Ane (P2D)). The Ane (U3D) is deployed to monitor the wind speeds in three orthogonal directions of u , v and w (see Fig. 3); whereas the Ane (P2D) is used to measure the wind velocities and wind directions in the horizontal plane (i.e., the u - v plane). The three orthogonal directions u , v and w are defined as: (i) u is the direction perpendicular to the alignment of the bridge deck; (ii) v is the direction parallel to the alignment of the bridge deck; and (iii) w is the direction perpendicular to the horizontal plane formed by u - v directions. The Ane (U3D) is deployed at deck-level in the middle of the main span on both the north and south sides as shown in Figs. 1(a) and 1(c); and the Ane (P2D) is deployed at tower-tops (one for each top) and deck-level in the middle of the Ma Wan side span on both the north and south sides, as shown in Fig. 1(a), where the figure in the parentheses denotes the number of the relevant sensors. A total of 110 dynamic strain gauges in three types, single strain sensor (SS), pair strain sensor (SP) and rosette strain sensor (SR), are installed at the structural components of three selected deck sections (including sections C and H in Fig. 1(a) and another one near section B), including chord members of the longitudinal trusses and cross frames, plan bracing members, deck through and rocker bearings at the Ma Wan tower, to measure the strain variation under different loadings. There are three types of accelerometers installed on the TMB: single-axial accelerometer (AS), bi-axial accelerometer (AB), and tri-axial accelerometer (AT). Four single-axial and four bi-axial accelerometers are deployed at sections B, D, F and G of the bridge deck (section B is at 1/2 of the Ma Wan side span; sections D, F and G are at 1/6, 1/3, and 1/2 of the main span, respectively), and one tri-axial accelerometer is installed at the Ma Wan abutment (see Fig. 1(a)). At each of the four deck sections B, D, F and G, one single-axial accelerometer is installed on the north side to measure acceleration in the vertical direction, while one bi-axial accelerometer is installed on the south side to measure the accelerations in both vertical and lateral directions. The level sensors which are sophisticated pile-line systems consisting of oil and water pipelines

throughout the bridge alignment are used to measure the vertical deflection and rotations of deck sections by pressure difference at measured locations (Wong 2004, Wong 2007, Ni *et al.* 2011). There are six level sensor stations at deck sections B, E and G, with two at each section (one on the north side and the other on the south side), as shown in Fig. 1(c); and one station at the Ma Wan abutment as a reference, to measure the vertical displacement of the deck. In addition to the level sensing stations, there are six GPS rovers on deck sections B, E and G to measure the displacement of the deck, as shown in Fig. 1(c).

4. Monitoring of dynamic strain caused by railway traffic

When a train passes through the TMB, the measured strain experiences a significant increase. The number of trains running on the bridge, the speed and location of the trains can be identified easily using the data from opposite strain gauges. In this study, strain data measured by the strain gauges SSTLN04 and SSTLS04 on the cross frame at section H (see Figs. 1(a) and 1(c)), near the north and south railway tracks respectively, are used to detect the passage of trains. When a train is passing section H on the north track, the strain at SSTLN04 would be under compression while the strain at SSTLS04 would be in tension. As a result, the strains measured by these two gauges would be opposite in plus-minus and the magnitude of the strain from SSTLN04 would be much larger than that from SSTLS04. When two trains pass section H side by side in opposite directions, the strains measured by SSTLN04 and SSTLS04 would be both compressive strain and the magnitudes would be roughly equal to each other.

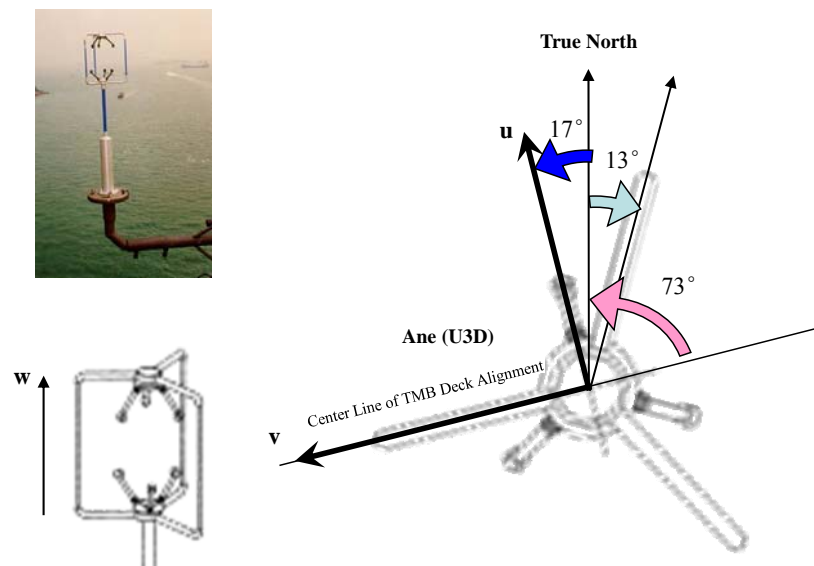


Fig. 3 Layout of Ane (U3D) on TMB

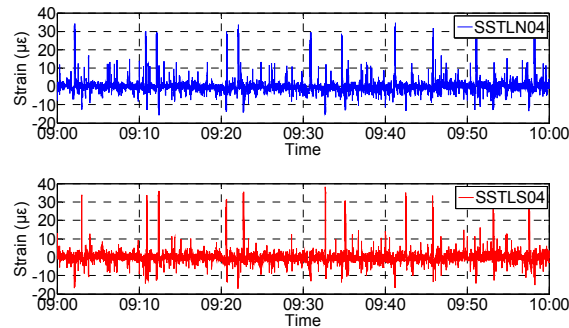


Fig. 4 Strain measured by strain gauges near the railway tracks

The strain time-histories measured by SSSLN04 and SSTLS04 respectively during the time interval 09:00-10:00 on 1 January 2012 are shown in Fig. 4 (the positive value is compressive strain and the negative value is tensile strain), in which the strain due to temperature has been eliminated by a wavelet-based method (Ni *et al.* 2012, Xia *et al.* 2012). The compressive strain more than 20 µε and obviously larger than others is induced by train; while the compressive strain much smaller is mainly induced by highway traffic. Three railway traffic cases: (i) no train on the bridge, (ii) one train running on the bridge, and (iii) two trains running in opposite directions on the bridge, will be identified using the time history of the strain as shown in Fig. 4. Considering the fact that it takes about 1.5 minutes for a train to pass through the whole bridge and the time lag for two trains running on the bridge, data segments in 3-minute duration for each will be used in the identification of the three railway traffic cases.

4.1 No train on bridge

It can be judged that there is no passage of train on the TMB during 09:05-09:08 according to Fig. 4. The corresponding time histories of strain from SSSLN04 and SSTLS04 are illustrated in Fig. 5. In this time slot, the maximum compressive and tensile strains measured by SSSLN04 are 14.3 µε and 6.4 µε, respectively; and the maximum compressive and tensile strains measured by SSTLS04 are 8.4 µε and 8.6 µε, respectively.

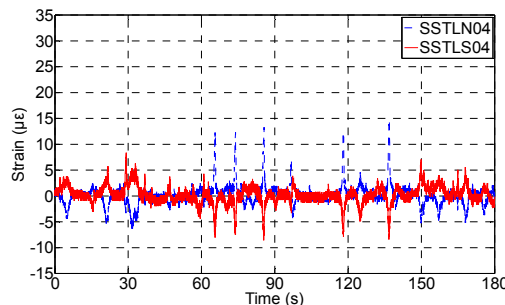


Fig. 5 Strain time histories when no train passes through TMB

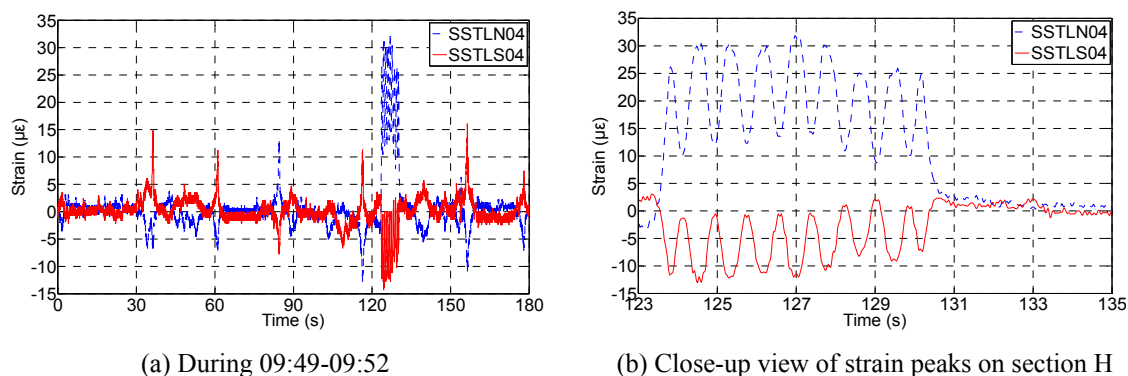


Fig. 6 Strain time histories when one train passes through TMB

4.2 One train running on bridge

From Fig. 4 it can be found that there is one train running on the TMB between 09:49 and 09:52. The corresponding time histories of strain measured by SSTLN04 and SSTLS04 including a close-up view of strain peaks at section H are shown in Fig. 6, in which there is a flock of strain peaks in a duration of about 7 s which is the time for the train to pass section H (where SSTLN04 and SSTLS04 are installed); the peaks measured by SSTLN04 are positive (compressive strain) while those measured by SSTLS04 are negative (tensile strain), and the absolute peak values from SSTLN04 are greatly larger than those from SSTLS04, indicating that the train was running on the north track. Furthermore, it can be judged from Fig. 6(b) that the passing train was an 8-car train because nine peaks were detected (two peaks for the bogies at the head and end of the train individually, and seven peaks for the fourteen bogies which can be divided into seven groups with every two close to each other, see Fig. 2). Therefore, the features which can be used to identify the passage of a train on the TMB are: (1) there is a flock of peaks with values higher than $20 \mu\epsilon$, noticeably larger than others; and (2) the number of the strain peaks in the peak flock is most probably eight for the data before 2003, nine for the data after 2005, and eight or nine for the data between 2003 and 2005, according to the characteristics of the trains passing through the TMB. The total length of an 8-car train is approximately 182 m, and as shown in Fig. 6, the time for the train passing section H is about 7.0 s; as a result, the speed of the train is approximately 26.0 m/s. Assuming that the speed of the train was constant when it ran on the TMB, it can be deduced that the train arrived at the Ma Wan side of the TMB at 09:50:06, reached section H at 09:51:03 and totally ran out of the TMB at the Tsing Yi side at 09:51:35. When the train passed section H, the maximum compressive strain measured by SSTLN04 was $32.1 \mu\epsilon$ and the maximum tensile strain measured by SSTLS04 was $14.4 \mu\epsilon$.

4.3 Two trains running in opposite directions on bridge

The close-up view of the strain measured by SSTLN04 and SSTLS04 during 09:45-09:48 is shown in Fig. 7. There is one salient peak flock of compressive strain between 09:45 and 09:48 for strain time histories measured by both SSTLN04 and SSTLS04, and the two peak flocks are quite close to each other. It can be concluded that there were two trains, one on the north track and the

other on the south track, running on the TMB during this time period, and they arrived and left section H nearly at the same time, i.e., they passed section H side by side. From Fig. 7(b) it can be observed that the peak flock from SSTLS04 emerges earlier than that from SSTLN04. The train on the south railway track arrived at section H first (0.3 s earlier than the train on the north track); and also the peak flock from SSTLS04 disappeared first, implying that the train on the south track left section H earlier (1.1 s earlier than the train on the north track). In addition, when arriving at section H, the train on the north track was just about half a car behind; however, when leaving this section, the train on the north track was 1.5 cars behind. It means that the speed of the train on the north track was lower than that of the train on the south track because the two trains were both of 8-car and their total lengths are equal to each other. It takes 6.4 s and 5.4 s for the trains on the north and south tracks to pass section H respectively, and the corresponding speed of the trains was 28.4 m/s and 33.7 m/s respectively, i.e. the speed of the train on the north track was slower than that of the train on the south track by 5.3 m/s. Assuming that the speeds of the two trains were constant when running on the TMB, it can be deduced that the train on the south track arrived at the Tsing Yi side of the TMB at 09:45:28, reached section H at 09:45:48, and totally ran out of the TMB at 09:46:33; while the train on the north track arrived at the Ma Wan side of the TMB at 09:44:56, met with the train on the south track at section H at 09:45:49 and totally ran out of the TMB at 09:46:12. When the two trains pass section H, the maximum compressive strain values measured by SSTLN04 and SSTLS04 are 31.9 $\mu\epsilon$ and 33.4 $\mu\epsilon$, respectively.

5. Torsional response

It is anticipated that there would be torsional response of the bridge deck under various loadings, especially when a train passes through the bridge or the bridge is stricken by a typhoon. The torsional response is likely to induce flutter of the bridge and/or deform the railway track on the bridge deck, adversely affecting the comfort of passengers and even threatening the running safety of trains. Therefore, the torsional dynamic response of the bridge deck is evaluated in the present study by using the long-term structural health monitoring data collected by the WASHMS.

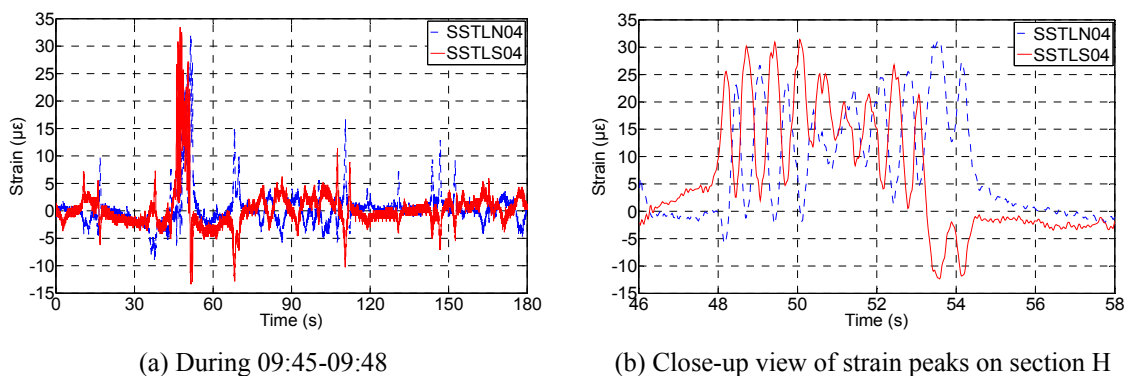


Fig. 7 Strain time histories when two trains pass by TMB

5.1 Weak wind condition

Weak wind condition is the case when the hourly mean wind speeds measured by the two Anes (U3D) at deck-level of section G on both the north and south sides (see Figs. 1(a) and 1(c)) are less than 2 m/s. The hourly mean wind speeds in the three orthogonal directions of u , v and w (see Fig. 3) are calculated by

$$\bar{U}_u = \frac{1}{T} \int_0^T U_u(t) dt = \frac{1}{N} \sum_{i=1}^N U_u(t_i) \quad (1)$$

$$\bar{U}_v = \frac{1}{T} \int_0^T U_v(t) dt = \frac{1}{N} \sum_{i=1}^N U_v(t_i) \quad (2)$$

$$\bar{U}_w = \frac{1}{T} \int_0^T U_w(t) dt = \frac{1}{N} \sum_{i=1}^N U_w(t_i) \quad (3)$$

where T is the time duration for calculating wind speed, and $T = 3,600$ s here to obtain hourly mean wind speed; $N = T/\Delta t = T f_s$ is the number of data obtained in one hour, in which Δt is the time interval and f_s is the sampling rate of wind data, 2.56 Hz. The hourly mean wind speed can be determined by

$$\bar{U} = \sqrt{\bar{U}_u^2 + \bar{U}_v^2 + \bar{U}_w^2} \quad (4)$$

Fig. 8 illustrates the wind speeds in the three orthogonal directions of u , v and w measured by the Ane (U3D) at section G on the south side during the period of 09:00-10:00 on 1 January 2012, and the corresponding hourly mean wind speed is calculated to be 1.4 m/s according to Eqs. (1)-(4).

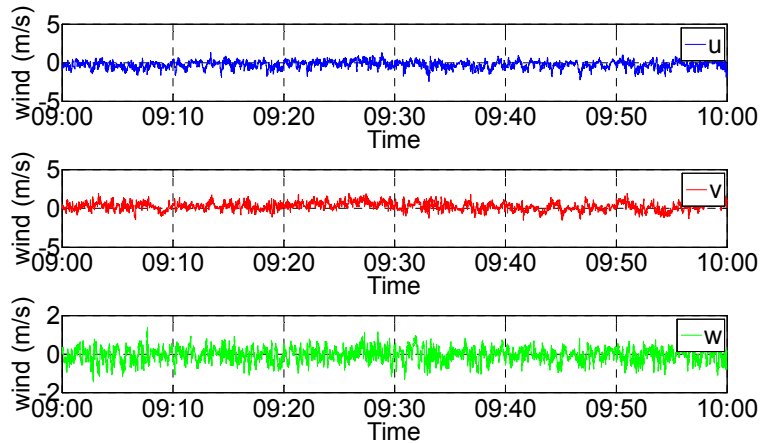


Fig. 8 Wind speeds in u , v and w directions measured by Ane (U3D) at section G under weak wind

Since the frequency of the dynamic displacement response of the bridge deck due to railway traffic is significantly lower than that due to highway traffic and wind loads, a cut-off frequency can be applied to the time histories of the displacement data to extract the displacement due to railway loads. This cut-off frequency is adopted as 0.08 Hz by trial-and-error. Therefore, a low-pass filter with an upper bound frequency of 0.08 Hz is applied to the time histories of the vertical dynamic displacement of the bridge deck to eliminate the influence of wind and highway traffic.

The time histories of the vertical displacements measured by the level sensing stations in the three railway traffic cases are shown in Figs. 9-11, respectively. Fig. 9 shows the time histories of the vertical displacements at sections B, E, and G on both the north and south sides and the reference vertical displacement at the Ma Wan abutment when there is no train running on the bridge. Even when there is no passage of a train, the recorded displacement at sections A, B, E, and G is still not equal to zero, implying that the effect of other factors cannot be completely excluded by the low-pass filter. However, the displacement is small and the maximum vertical values at sections B, E, and G are all less than 60.0 mm. Fig. 10 shows the time histories of the vertical displacements at sections B, E, and G on both the north and south sides and the reference vertical displacement at the Ma Wan abutment when there is one train running on the bridge. The train is detected to be running on the north railway track directed from Ma Wan to Tsing Yi, which means that the train passed sections B, E, and G successively, and what shown in Fig. 10 coincides with this judgment because the vertical displacements measured by the level sensing stations at sections B, E and G reach their maximum absolute values one after another in accordance with the passing-by of the train. Fig. 11 illustrates the time histories of the vertical displacements at sections B, E, and G on both the north and south sides and the reference vertical displacement at the Ma Wan abutment when there are two trains running on the bridge. Coinciding with the inference from the strain measured by SSTLN04 and SSTLS04, one train is running on the north railway track heading toward the Tsing Yi side, inducing the left peak-trough in Figs. 11(b)-11(d), while the other train is running on the south railway track heading toward the Ma Wan side, inducing the right peak-trough in Figs. 11(d). The left peak-trough moved from section B to section G over time, whereas the right peak-trough moved in a contrary direction over time; they meet with each other at section H, so they are most close to each other at section G among the sections deployed with level sensing stations. From Figs. 10-11 it can be seen that apart from downward displacement induced by static load, the train also generates relatively large upward displacement, implying that the running train made the bridge deck to vibrate. In addition, it is found that the vertical displacement at section E is obviously larger than that at section G which can be explained by the mode shape of the main deck. The first vertical mode of the main deck is almost asymmetric in the main span (Ni *et al.* 1999), so the vertical deflection at 1/4 span, i.e., section E, is the maximum one. When the train passes through the TMB, the maximum downward displacement on the north and south sides of section E is 305.3 mm and 282.8 mm, respectively, with a difference of 22.5 mm; and the maximum downward displacement on the north and south sides of section G is 243.8 mm and 229.3 mm, respectively, with a difference of 14.5 mm. When the two trains pass by the TMB, the maximum downward displacement on the north and south sides of section E is 390.5 mm and 421.4 mm, respectively, with a difference of 30.9 mm; and the maximum downward displacement on the north and south sides of section G is 345.0 mm and 363.2 mm, respectively, with a difference of 18.2 mm. The vertical displacement of the north and south sides of the deck is almost symmetric because the differences between the measured displacements on both sides are small (less than 40.0 mm).

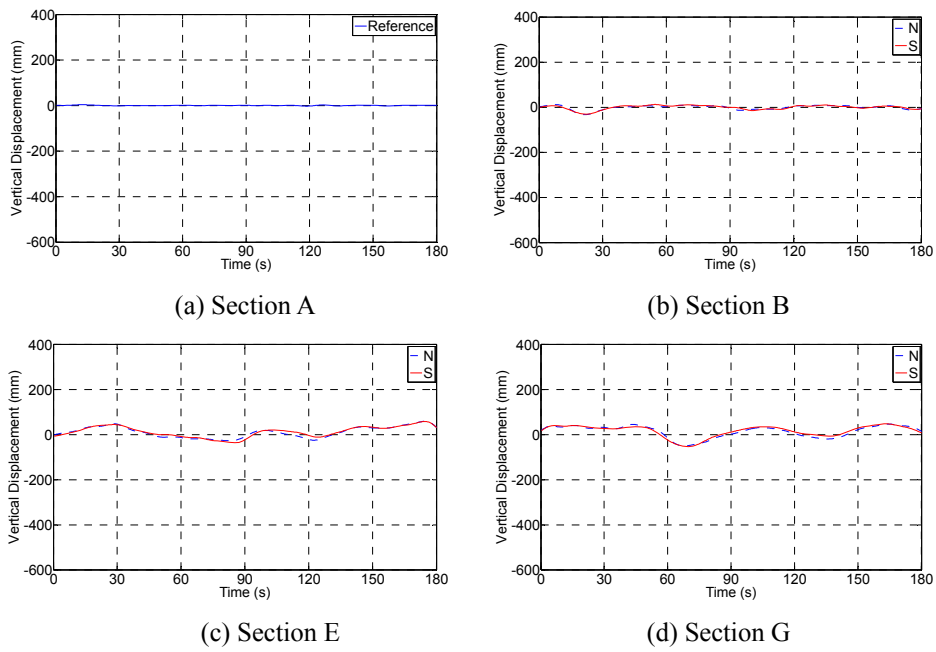


Fig. 9 Time histories of vertical displacement when no train passes through TMB

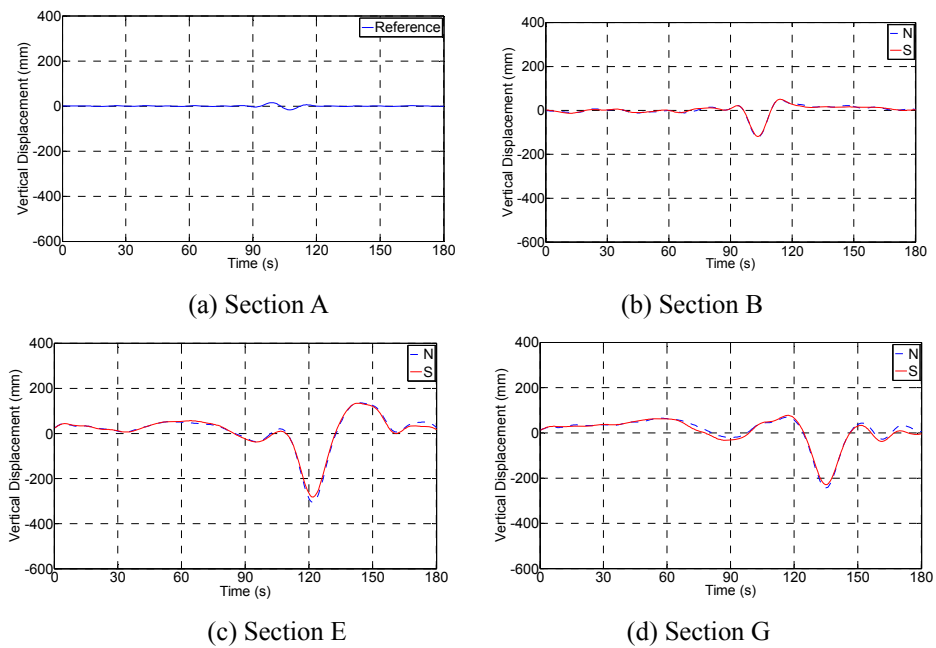


Fig. 10 Time histories of vertical displacement when one train passes through TMB

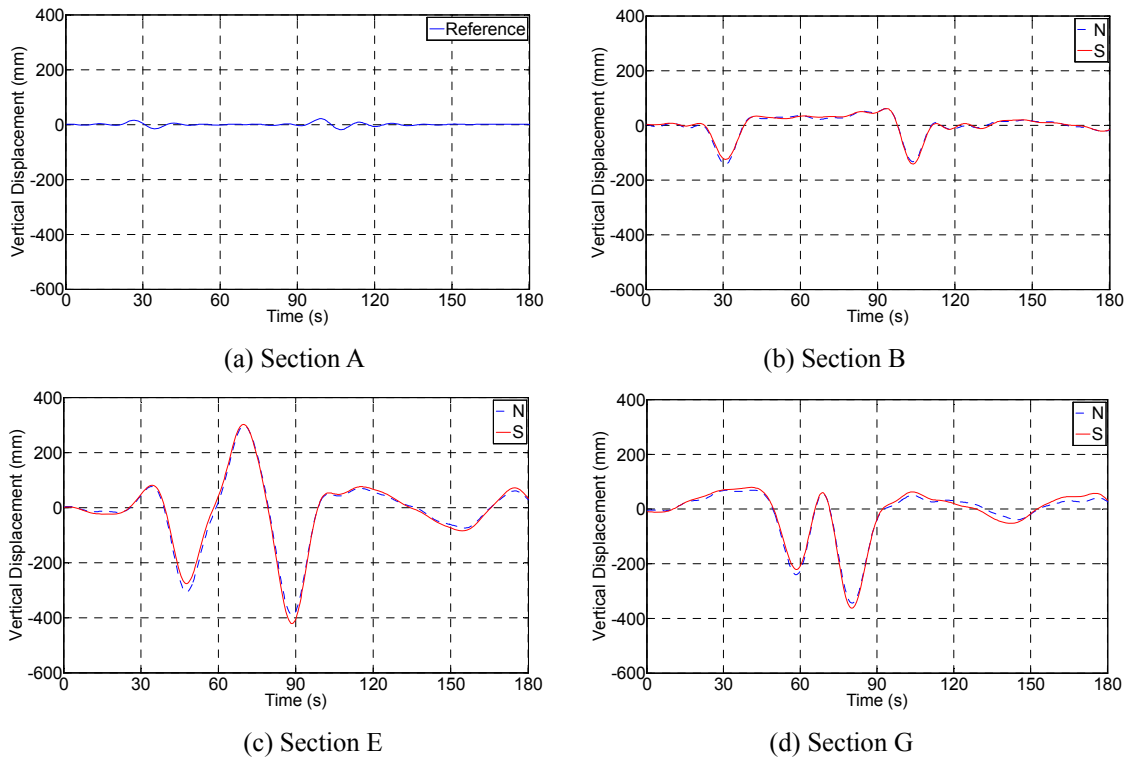


Fig. 11 Time histories of vertical displacement when two trains pass through TMB

The rotation angles of sections E and G are obtained by dividing the difference between the vertical displacements on the north and south sides of the deck by the distance between the two sensors on the same section (see Fig. 1(c)). That is

$$R = \frac{\arctan((D_n - D_s) / B)}{\pi} \times 180 \tag{5}$$

where R is the rotation angle of the deck, in the unit of degree; D_n and D_s are the vertical displacement on the north and south sides of the deck measured by the level sensing stations, respectively; and B is the distance between the two sensors which is 30.05 m for the level sensing stations.

The derived time histories of the rotation angles of sections E and G in the three railway traffic cases are shown in Figs. 12-14. As mentioned above, the influence of other factors cannot be completely excluded from the vertical displacement induced by trains merely by the low-pass filter, so there is still rotation at sections E and G when there is no train running on the bridge. It can be seen in these figures that the passage of train exaggerates the rotation of the deck but the increase is not so significant, and the rotation angles of the deck at sections E and G are less than 0.05° when one train passes through the TMB. In order to verify the credibility of the above conclusion, the data acquired on 1 February, 1 March, 1 April, 1 May, 2 June, 3 July, 3 August, 9 September,

22 October, 11 November and 10 December 2012 are arbitrarily selected and analyzed in the same way. What observed from these data is similar to that obtained from the data on 1 January 2012. It is found that the differences of the vertical displacements on the two opposite sides at sections E and G are all less than 60 mm.

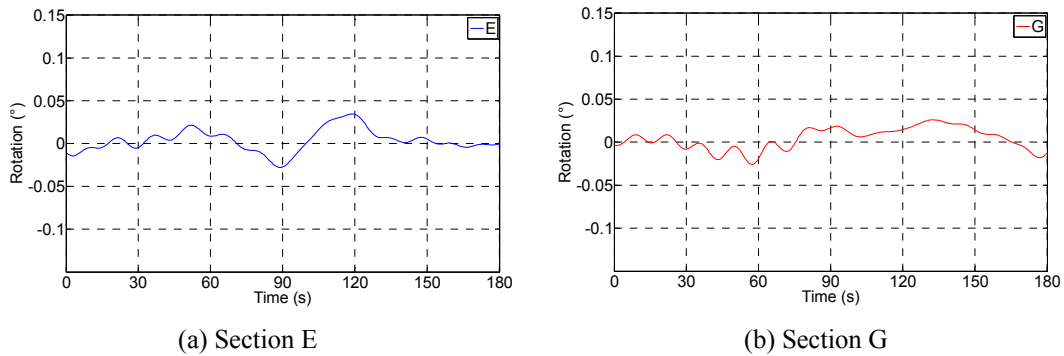


Fig. 12 Time histories of rotation angles when no train passes through TMB

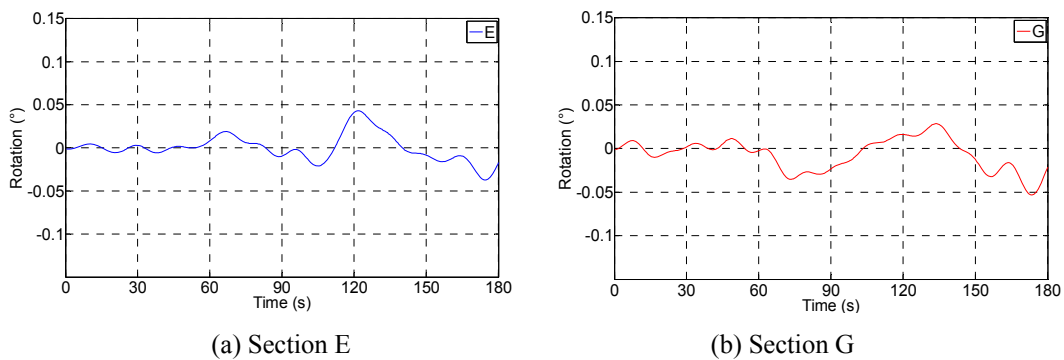


Fig. 13 Time histories of rotation angles when one train passes through TMB

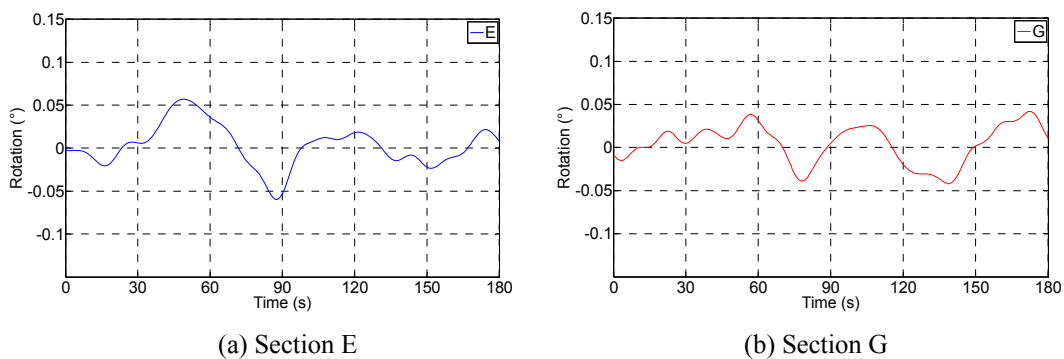


Fig. 14 Time histories of rotation angles when two trains pass through TMB

The histograms of the rotation angles of sections E and G in the three railway traffic cases are shown in Figs. 15-17. For comparison and validation, the vertical displacements measured by the GPS and the vertical displacements derived by integrating the acceleration data are also obtained. The vertical displacements on the opposite sides at the central mid-span (section G) obtained by the three approaches (level sensing stations, GPS, integration of acceleration data) when one train and two trains pass through the TMB during 09:00-10:00 on 2 June 2012, are shown in Fig. 18. When one train passes through the TMB, the maximum downward vertical displacement on the north side of the deck measured by the level sensing stations, GPS, and accelerometers (after integration twice) is 267.2 mm, 300.6 mm, and 239.2 mm, respectively; and that on the south side is 238.3 mm, 268.7 mm and 236.6 mm, respectively. The maximum rotation of the deck at section G measured by these three types of sensors is 0.06° , 0.07° , and 0.06° , respectively. In the case of two trains passing through the TMB, the maximum rotation of the deck at section G measured by the three types of sensors is 0.07° , 0.05° , and 0.08° , respectively. The rotation angles of sections E and G measured by the three types of sensors are all less than 0.1° in the three railway traffic cases and sometimes the exaggeration effect of the running train on the rotation angle of the deck is even not obvious at all, which means that the railway traffic alone is not fierce enough to evoke serious torsional dynamic displacement of the bridge deck.

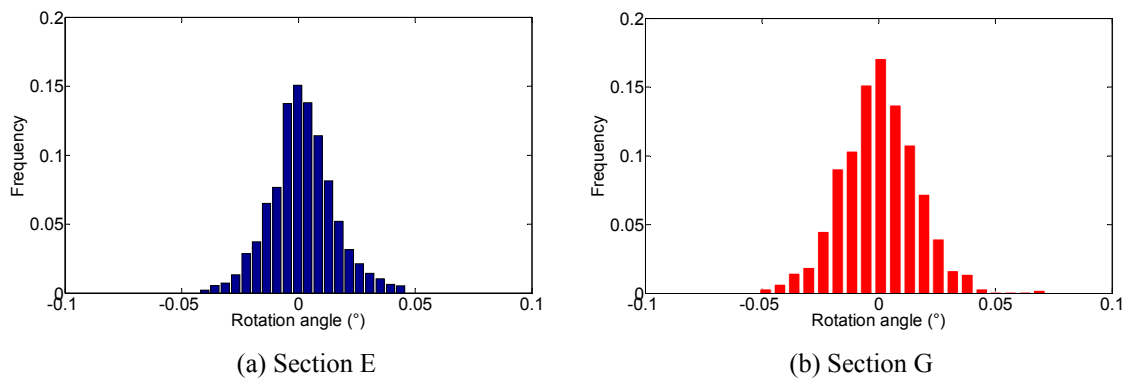


Fig. 15 Histograms of rotational angles when no train passes through TMB

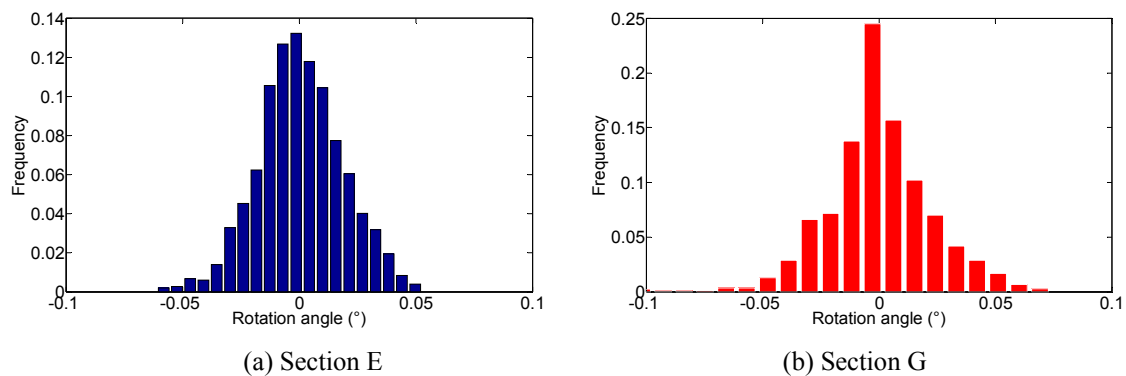


Fig. 16 Histograms of rotational angles when one train passes through TMB

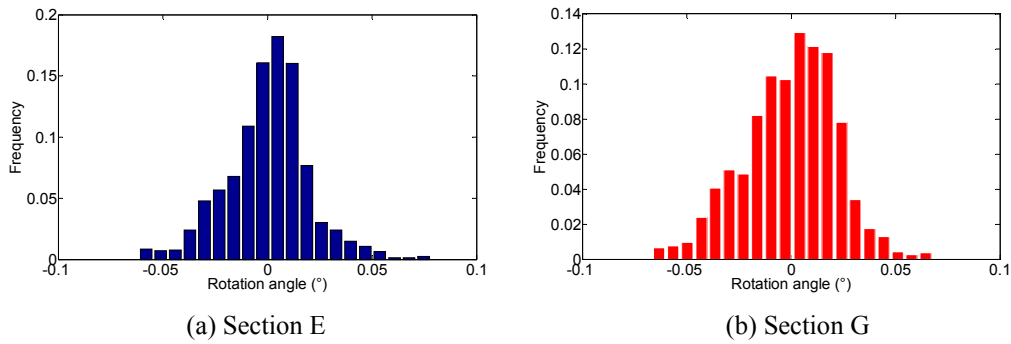


Fig. 17 Histograms of rotation angles when two trains pass through TMB

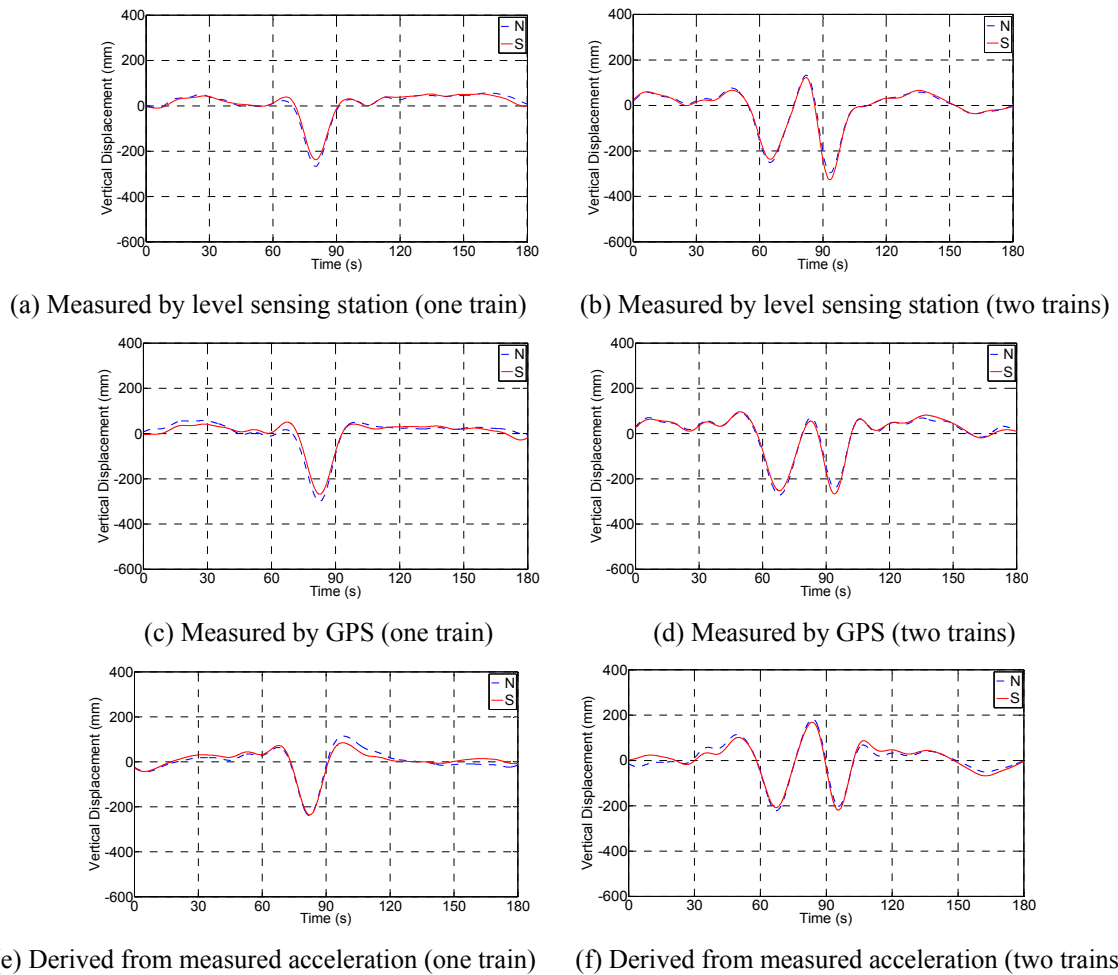


Fig. 18 Vertical displacements measured by level sensing stations, GPS, and accelerometers (after integration twice) when one train and two trains pass through TMB

5.2 Typhoon condition

Three typhoons with signal number no less than eight struck Hong Kong in 2012, namely, tropical storm Doksuri with signal No. 8 in June, typhoon Kai-tak with signal No. 8 in August, and severe typhoon Vicente with signal No. 10 in July. Doksuri formed as a tropical depression over the western North Pacific about 1,280 km east of Manila on 26 June, and reached its peak intensity over the seas to the northeast of Luzon on 28 June with an estimated maximum sustained wind of 85 km/h near its center. It moved west-northwestwards across the Luzon Strait during the day and entered the South China Sea on the night. Doksuri moved across the northern part of the South China Sea at about 27 km/h towards the coast of Guangdong near the Pearl River Estuary on 29 June. Kai-tak formed as a tropical depression over the western North Pacific about 960 km east-northeast of Manila on 12 August and intensified into a tropical storm on the following day. Kai-tak moved across northern Luzon on 15 August, entered the northern part of the South China Sea that evening and intensified into a severe tropical storm. On 16 August, Kai-tak intensified further into a typhoon in the afternoon, reaching its peak intensity with an estimated maximum sustained wind of 120 km/h. Vicente formed as a tropical depression over the western North Pacific about 450 km northeast of Manila on 20 July and intensified into a tropical storm on the night of 21 July. Vicente intensified into a severe tropical storm on the small hours of 23 July and gradually turned to move northwestwards in the morning. It underwent intensification into a typhoon in the afternoon, with its eye clearly discernible on the Hong Kong Observatory's radar. Shortly afterwards, Vicente intensified rapidly to a severe typhoon over the South China Sea to the south-southwest of Hong Kong towards mid-night, reaching its peak intensity with an estimated maximum sustained wind of 155 km/h near its center. Vicente speeded up towards the region west of the Pearl River Estuary thereafter. Vicente necessitated the issuance of the first No. 10 Hurricane Signal in Hong Kong since Typhoon York in September 1999 (HKO 2014). As recorded by the Ane (U3D) at the middle span (section G) of the TMB, the maximum gust speed and the maximum hourly mean wind speed during Doksuri were 24.1 m/s and 9.3 m/s respectively which occurred between 00:00 and 01:00 on June 30; the maximum gust speed and the maximum hourly mean wind speed during Kai-tak were 20.9 m/s and 9.7 m/s respectively which occurred between 02:00 and 03:00 on August 17; and the maximum gust speed and the maximum hourly mean wind speed during Vicente were 43.5 m/s and 16.8 m/s respectively which occurred between 01:00 and 02:00 on July 24. The wind speeds in the three orthogonal directions of u , v and w measured by the Ane (U3D) at section G on the south side between 01:00 and 02:00 on July 24 during typhoon Vicente are shown in Fig. 19.

The maximum differences of the vertical displacements measured by the level sensing stations on the two opposite sides at sections E and G of the bridge deck during typhoon Vicente are 209.8 mm and 272.7 mm, respectively. The maximum rotation angle at section E is 0.40° , and that at section G is 0.52° . The recorded maximum rotation of the TMB deck is 1.2° during typhoon York (signal No. 10) in 1999. The dynamic rotation responses of sections E and G during the strongest period of typhoon Vicente are shown in Fig. 20 in comparison with the recorded maximum rotation. Compared with the rotation angles under typhoon Vicente, the rotation angles of sections E and G under weak wind condition, most of which is less than 0.05° , are quite small. In addition, during the period of typhoons with signal no less than eight all highway traffic is prohibited from using the upper-deck carriageways, and thus the effect of highway traffic on the rotation of the bridge deck during strong typhoons is negligible. As a result, the rotation angles of the deck during typhoons are mainly caused by the strong winds. From the strains measured by SSSLN04 and

SSTLS04, it is detected that single train passed through the TMB at time intervals 01:07-01:10, 01:21-01:24, 01:25-01:28, 01:35-01:38, and 01:46-01:49; and two trains passed by the TMB at time interval 01:02-01:05. However, it is difficult to identify the effect of the trains on the rotation response of the deck, which also implies that the rotation of the deck under typhoons is dominated by the strong winds. The maximum differences of the vertical displacements measured by the level sensing stations on the two opposite sides at sections E and G of the bridge deck are 94.4 mm and 120.6 mm respectively during typhoon Doksar, and 78.7 mm and 89.2 mm respectively during typhoon Kai-tak. Accordingly, the maximum rotation angles at sections E and G are 0.18° and 0.23° respectively during typhoon Doksar, and 0.15° and 0.17° respectively during typhoon Kai-tak. The histograms of the rotation at section G and the wind speed during the strongest periods of typhoons Doksar, Kai-tak, and Vivente are shown in Figs. 21-23. The maximum rotation angles at sections E and G measured by the three types of sensors (level sensing stations, GPS, and accelerometers) are all less than 1° during the three typhoons in 2012.

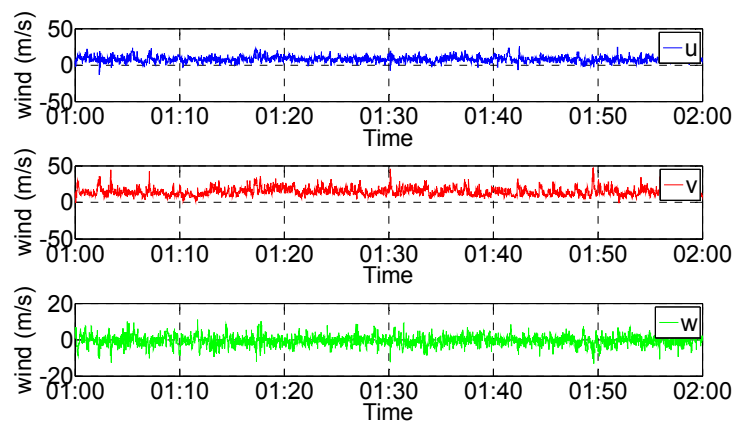


Fig. 19 Wind speeds in u, v and w directions measured by Ane (U3D) at section G during typhoon Vicente

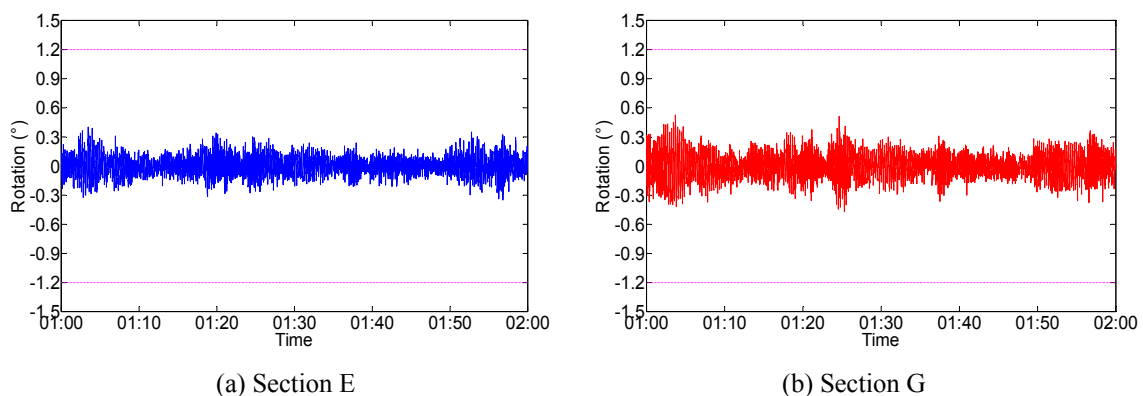


Fig. 20 Rotation responses at sections E and G during the strongest period of typhoon Vicente

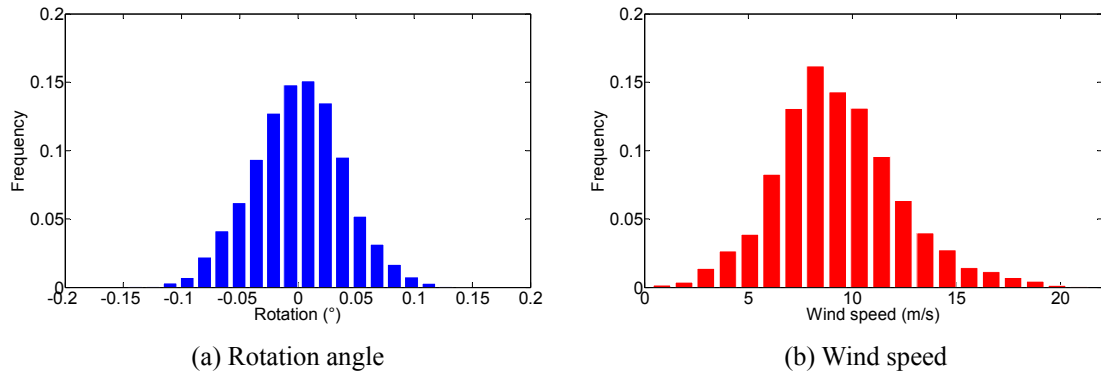


Fig. 21 Histograms of rotation at section G and wind speed during the strongest period of typhoon Doksuri

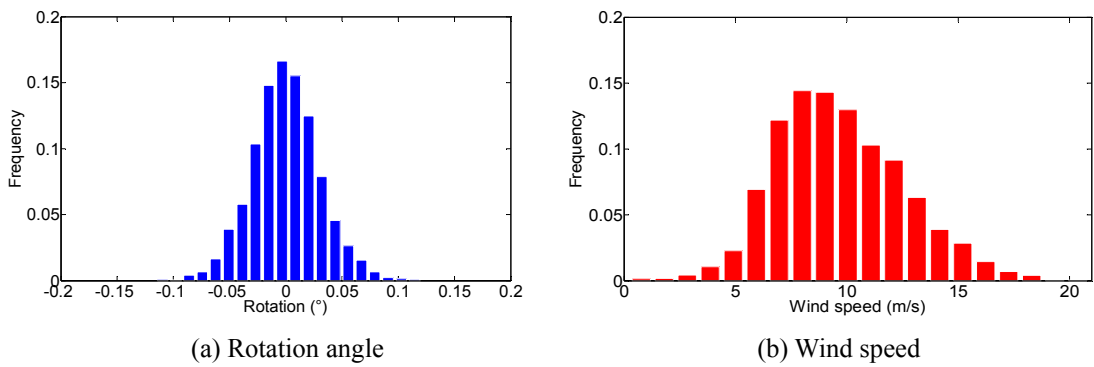


Fig. 22 Histograms of rotation at section G and wind speed during the strongest period of typhoon Kai-tak

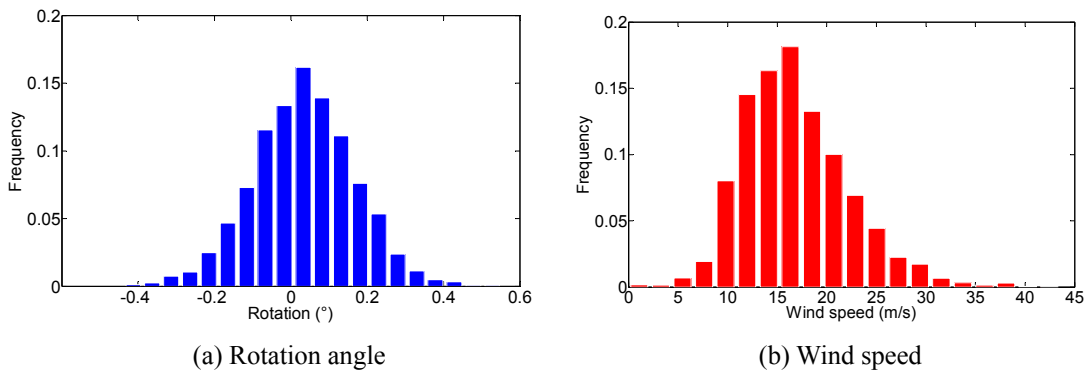


Fig. 23 Histograms of rotation at section G and wind speed during the strongest period of typhoon Vicente

It can be concluded that the rotation angle of the bridge deck is small either under railway traffic only or under both railway traffic and typhoon. The main span of the TMB is 1,377 m while the total length of the train traveling on the TMB is only 182 m, 13% of the main span length. Furthermore, the total weight of structural steel used in the deck is about 49,000 tons while the weight of the train is only about 400 tons and less than 1% of the weight of the steel deck. Therefore, the train is relatively short and light in comparison with the bridge deck. In addition, the two rail tracks on the TMB are located close to the longitudinal central line of the lower deck, weakening the effect of the running train on the torsional dynamic response of the bridge deck. As a result, under railway traffic only, the vertical displacements on the opposite sides of the bridge deck are nearly symmetric and the deck rotates little. Combining the main features of the deck types of the Fourth Road Bridge and the Seven Bridge, the TMB deck adopted double-deck box construction with truss stiffening and non-structural edge fairings. Longitudinal air vents were provided in the upper and lower surfaces to enhance aerodynamic stability. Aerodynamic testing of the bridge deck with wind inclination of up to ± 7.5 degree and assumption of structural damping coefficient of 0.03 confirmed the absence of divergent oscillations and examined vortex shedding oscillations (Beard and Young 1995). The wind inclinations of the three typhoons in 2012 are all in the range of -2.5 degree to 0 degree, so the critical wind speed is between 80 m/s and 99 m/s according to the aerodynamic testing results (Beard and Young 1995). The maximum wind speed during the three typhoons is 43.5 m/s observed during typhoon Vicente, which is much smaller than the critical wind speed. Therefore, the bridge deck was aerodynamically stable and the dynamic rotations were not significantly during the three typhoons in 2012.

6. Conclusions

The Tsing Ma Bridge (TMB) in Hong Kong is currently the world's longest suspension bridge carrying both highway and railway traffic and is located in a typhoon region. To study the torsional dynamic response of this bridge under railway traffic and strong winds, the unsymmetric vertical displacement and the rotation of the bridge deck under two environmental conditions (weak wind and typhoon conditions) and in three railway traffic cases (no train on the bridge, one train running on the bridge, two trains running in opposite directions on the bridge) are evaluated using one-year monitoring data acquired by a long-term structural health monitoring system deployed on the TMB. The wind conditions, railway traffic cases and rotation of the bridge deck are analyzed with the measurement data from strain gauges, anemometers, level sensing stations, GPS, and accelerometers. The analysis comes to the following conclusions:

- The strain data obtained from the strain gauges are effective and reliable to identify the railway traffic;
- The torsional dynamic response of the bridge deck due to railway traffic is negligible because the train is relatively short and light in comparison with the bridge deck;
- The torsional dynamic response of the bridge deck during typhoons is mainly caused by strong winds, and the torsion is small (less than 1 degree) due to the rational design of the bridge (e.g., adopting the stiffening deck system composed of a streamlined box-shaped steel truss girder with central air-gap); and
- The long-term structural health monitoring system deployed on the TMB was still working well after 15 years of operation (up to 2012).

Acknowledgments

The work described in this paper was supported by a grant from the Research Grants Council of the Hong Kong Special Administrative Region, China (Project No. PolyU 5224/13E) and a grant from the National Science Foundation of China (Grant No. U1234201). The writers also wish to thank the Hong Kong SAR Government Highways Department for providing the long-term structural health monitoring data of the Tsing Ma Bridge.

References

- Beard, A.S. and Young, J.S. (1995), "Aspect of the design of the Tsing Ma Bridge", *Proceedings of the International Conference on Bridges into 21st Century*, Hong Kong.
- Boonyapinyo, V., Miyata, T. and Yamada, H. (1999), "Advanced aerodynamic analysis of suspension bridges by state-space approach", *J. Struct. Eng. - ASCE*, **125**(12), 1357-1366.
- Cai, C.S. and Chen, S.R. (2004), "Framework of vehicle-bridge-wind dynamic analysis", *J. Wind Eng. Ind. Aerod.*, **92**(7), 579-607.
- Chen, X., Matsumoto, M. and Kareem, A. (2000), "Time domain flutter and buffeting response analysis of bridges", *J. Eng. Mech. - ASCE*, **126**(1), 7-16.
- Chen, X. and Kareem, A. (2003), "Aeroelastic analysis of bridges: effects of turbulence and aerodynamic nonlinearities", *J. Eng. Mech. - ASCE*, **129**(8), 885-895.
- Diana, G. and Cheli, F. (1989), "Dynamic interaction of railway systems with large bridges", *Vehicle Syst. Dyn.*, **18**(1-3), 71-106.
- Diana, G., Rocchi, D., Argentini, T. and Muggiasca, S. (2010), "Aerodynamic instability of a bridge deck section model: linear and nonlinear approach to force modeling", *J. Wind Eng. Ind. Aerod.*, **98**(6), 363-374.
- Ding, Q., Lee, P.K.K. and Lo, S.H. (2000), "Time domain buffeting analysis of suspension bridges subjected to turbulent wind with effective attack angle", *J. Sound Vib.*, **233**(2), 311-327.
- Fryba, L. (1996), *Dynamics of Railway Bridges*, Vol. 1, Thomas Telford, London, UK.
- Guo, W.W., Xia, H., Zhang, T. and Sun, G.J. (2011). "Dynamic responses of a railway bridge under high-speed trains subjected to turbulent winds", *Proceedings of the 8th International Conference on Structural Dynamics*, Leuven, Belgium.
- Hong Kong Observatory (HKO), *Hong Kong's tropical cyclone warning signals*, <<http://www.hko.gov.hk/contentc.htm>> (February 28, 2014).
- Hong Kong Observatory (HKO), *Tropical Cyclones Affecting Hong Kong in 2012*, <<http://www.hko.gov.hk/contentc.htm>> (February 28, 2014).
- Kwark, J.W., Choi, E.S., Kim, Y.J., Kim, B.S. and Kim, S.I. (2004), "Dynamic behavior of two-span continuous concrete bridges under moving high-speed train", *Comput. Struct.*, **82**(4), 463-474.
- Larose, G.L., and Livesey, F.M. (1997), "Performance of streamlined bridge decks in relation to the aerodynamics of a flat plate", *J. Wind Eng. Ind. Aerod.*, **69**, 851-860.
- Larsen, A. (2000), "Aerodynamics of the Tacoma Narrows Bridge-60 years later", *Struct. Eng. Int.*, **10**(4), 243-248.
- Lee, C.H., Kim, C.W., Kawatani, M., Nishimura, N. and Kamizono, T. (2005), "Dynamic response analysis of monorail bridges under moving trains and riding comfort of trains", *Eng. Struct.*, **27**(14), 1999-2013.
- Ni, Y.Q., Ko, J.M. and Wang, J.Y. (1999), *Finite element modelling and modal sensitivity analysis of the Tsing Ma Suspension Bridge*, Report No. 3(a), Department of Civil and Structural Engineering, The Hong Kong Polytechnic University, Hong Kong.
- Ni, Y.Q., Wong, K.Y. and Xia, Y. (2011), "Health checks through landmark bridges to sky-high structures", *Adv. Struct. Eng.*, **14**(1), 103-119.

- Ni, Y.Q., Xia, H.W., Wong, K.Y. and Ko, J.M. (2012), "In-service condition assessment of bridge deck using long-term monitoring data of strain response", *J. Bridge Eng. - ASCE*, **17**(6), 876-885.
- Pfeil, M.S. and Batista, R.C. (1995), "Aerodynamic stability analysis of cable-stayed bridges", *J. Struct. Eng. - ASCE*, **121**(12), 1784-1788.
- Scanlan, R.H. (1978), "The action of flexible bridges under wind, II: Buffeting theory", *J. Sound Vib.*, **60**(2), 201-211.
- Scanlan, R.H. and Jones, N.P. (1990), "Aeroelastic analysis of cable-stayed bridges", *J. Struct. Eng. - ASCE*, **116**(2), 279-297.
- Wong, K.Y. (2004), "Instrumentation and health monitoring of cable-supported bridges", *Struct. Control Health. Monit.*, **11**(2), 91-124.
- Wong, K.Y. (2007), "Design of a structural health monitoring system for long-span bridges", *Struct. Infrastruct. E.*, **3**(2), 169-185.
- Wu, T. and Kareem, A. (2013), "Bridge aerodynamics and aeroelasticity: A comparison of modeling schemes", *J. Fluid. Struct.*, **43**, 347-370.
- Xia, H., Guo, W.W., Zhang, N. and Sun, G.J. (2008). "Dynamic analysis of a train-bridge system under wind action", *Comput. Struct.*, **86**(19), 1845-1855.
- Xia, H.W., Ni, Y.Q., Wong, K.Y. and Ko, J.M. (2012), "Reliability-based condition assessment of in-service bridges using mixture distribution models", *Comput. Struct.*, **106-107**, 204-213.
- Xu, Y.L., Guo, W.W., Chen, J., Shum, K.M. and Xia, H. (2007), "Dynamic response of suspension bridge to typhoon and trains. I: field measurement results", *J. Struct. Eng. - ASCE*, **133**(1), 3-11.
- Zhai, W., Xia, H., Cai, C., Gao, M., Li, X., Guo, X. and Wang, K. (2013), "High-speed train-track-bridge dynamic interactions-Part I: theoretical model and numerical simulation", *Int. J. Rail Transport.*, **1**(1-2), 3-24.